https://doi.org/10.5194/amt-2021-55
Preprint. Discussion started: 18 March 2021

Atmospheric Measurement Techniques
Discussions

Atmospheric Optical Turbulence Profile Measurement and Model Improvement over Arid and Semi-arid regions

Hao Yang[1,2,3], Zhiyuan Fang[1,2,3], Cheng Li[1,2,3], Xu Deng[1,2,3], Kunming Xing[1,3], Chenbo Xie[1,3*]

[1] Key Laboratory of Atmospheric Optics, Anhui Institute of Optics and Fine Mechanics, Chinese Academy of Sciences, Hefei 230031, China

[2] Science Island Branch of Graduate School, University of Science and Technology of China, Hefei 230026, China

[3]Advanced Laser Technology Laboratory of Anhui Province, Hefei 230037, China

*** Corresponding author:** Chenbo Xie (cbxie@aiofm.ac.cn)

Abstract: From August 4th to 30th, 2020 and from November 27th to December 25th, 2020, a self-developed radiosonde balloon system was used to observe high-altitude atmospheric optical turbulence at three sites in northwestern China, and an improved model based on the observational data was established. Through comparative analysis of the observational data and the improved model, the distribution characteristics of atmospheric optical turbulence under the combined action of different meteorological parameters and different landform features in different seasons were obtained. The improved model can show the variation of the detailed characteristics of turbulence with the height distribution, and the degree of correlation with the measured values is above 0.82. The improved model can provide a theoretical basis and supporting data for turbulence estimation and forecasting in northwestern China.

Keywords: optical turbulence observation, improved model, turbulence estimation.

1. Introduction

The atmospheric refractive index structure constant (C_n^2) is commonly used to characterize atmospheric optical turbulence, and its distribution with height is called the atmospheric optical turbulence profile (Hutt, 1999; Wu et al., 2007). As light waves propagate in the atmosphere, they are affected by atmospheric optical turbulence, resulting in light-intensity flicker, image-point jitter, and image blurring, which affect the performance of photoelectric systems (e.g., the decline in the observation level of astronomical telescopes, the interference of laser transmission, the degradation of optical remote sensing imaging quality) (Bendersky et al., 2004; Bi et al., 2020; He et al., 2008; Rani et al., 2019). Therefore, obtaining the atmospheric optical turbulence profile is essential for improving the performance of optical systems. Various methods and instruments are used to measure C_n^2; however, existing measurements are extremely limited in time and space (Kornilov et al., 2007; Osborn et al., 2017; Travouillon et al., 2011; Wu et al., 2007). Research on forecasting high-altitude atmospheric optical turbulence, while meeting a certain accuracy, can not only resolve these time and space limitations of measurement methods, but also meet the needs of engineering applications. It is an effective method to obtain the atmospheric optical turbulence parameters, which can eliminate the limitation of the measurement environment. For example, the Mauna Kea Observatory in Hawaii, USA, has carried out work on forecasting atmospheric optical turbulence at high altitude, improving the efficiency of the

https://doi.org/10.5194/amt-2021-55
Preprint. Discussion started: 18 March 2021

Atmospheric Measurement Techniques Discussions

telescope (Cherubini et al., 2008).

Much work has been carried out by researchers on the parameterization and model forecasting of atmospheric optical turbulence. The Tatarski model established a relationship between atmospheric optical turbulence and meteorological parameters (Tatarski, 1961). Hufnagel et al.(1964) proposed a single-parameter, mid-latitude model, which was limited in its scope of use. Van Zandt et al. (1981) statistically processed the fine structure of the atmosphere and proposed a random model, which was more complex but not very satisfactory. Other researchers have estimated atmospheric optical turbulence profiles through the relationship between outer scale and meteorological parameters (Basu, 2015; Wu et al., 2020a). Dewan et al. (1993) proposed an outer-scale model (Dewan model) including wind shear factors through a large number of experimental observations. Through experiments, Ruggiero et al. (2004) further derived an outer-scale model (HMNSP99 model) incorporating both wind shear and temperature gradients.

To avoid the impact of optical turbulence on site selection of observatories, astronomers all over the world are looking for suitable sites for astronomical observations. Northwestern China has a typical arid climate, with special terrain such as plateaus, deserts, mountains, and Gobi deserts, which has attracted the attention of many scientists. To date, research on the characteristics of turbulence in northwestern China has been carried out in only a few areas, such as Ali, Dachaidan, and Lhasa (Bi et al., 2020; Wang et al., 2013; Wu et al., 2020a; Wu et al., 2020b). Therefore, further research on turbulence parameters in northwestern China is still needed.In this study, a month-long turbulence observation campaign was carried out at three typical observation sites (Golmud, Dunhuang, and Zhangye) in northwestern China. Golmud is located in the hinterland of the Qinghai-Tibet plateau, with an average elevation of 2780 m, and its climate is a typical plateau climate. There are mountains, Gobi deserts, wind-eroded hills, alpine plains, salt lakes, and other special types of terrain in Golmud City. Zhangye (average altitude of 1485 m) and Dunhuang (average altitude of 1140 m) are located in the middle and at the western end of the Hexi Corridor, respectively. They are important economic cities on the Silk Road and are home to several special terrain types and landforms, such as mountains, deserts, and Gobi deserts. In addition to the arid climate, there is also a special semi-arid and semi-humid climate in the Qilian Mountain alpine zone. These typical geographic and climatic characteristics are useful for studying the rich characteristics of turbulence.

In this paper, the turbulence distribution characteristics in summer and winter at three sites in a typical area of northwestern China are investigated based on the results of long-term turbulence observations. The empirical models representing each site were fitted based on the Hufnagel–Vally model, and these models could represent the general variation pattern of turbulence over each site. Furthermore, the HMNSP99 model was improved by refitting the limited observational data. The improved model can be well matched with the climate and geographical environment of the observation sites.

2. Data and methods

2.1 Radiosonde data

Sounding experiments were conducted during the period Aug. 4–30, 2020 and Nov. 27 to Dec. 25, 2020, at Golmud Meteorological Observatory (N: 36.4, E: 94.9), Dunhuang Meteorological Observatory (N: 40.14, E: 94.6), and Zhangye Meteorological Observatory (N:

38.9, E: 100.4), using the radiosonde developed by the Anhui Institute of Optics and Fine Mechanics, Chinese Academy of Sciences. The records of the radiosonde balloon (hereinafter referred to simply as 'the balloon') released during the experiment are shown in Table 1. The radiosonde was tied under the balloon with a rope length of 60 m (to avoid the balloon disturbing the measurement accuracy). The balloon was expanded to drive the load up with an average lift speed of 6 m/s. It was released each morning and night, and 52 balloons were released at each site, with an effective sounding balloon count of 145.

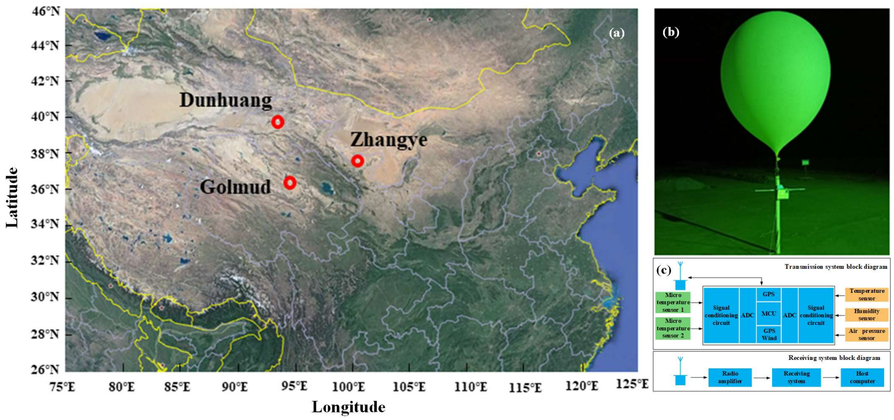

Figure 1. Atmospheric optical turbulence measurement at three sites in northwestern China: (a) map (Satellite images from © Google Earth 2021) showing the locations of the sites—namely, Golmud (N: 36.4, E: 94.9) at altitude 2780 m, Dunhuang (N: 40.14, E: 94.6) at altitude 1140 m, and Zhangye (N: 38.9, E: 100.4) at altitude 1485 m; (b) the radiosonde balloon equipment; (c) schematic circuit diagram of the radiosonde balloon system.

Table 1. Records of radiosonde balloons released at the three sites in this study.

Location	Altitude	Launch dates	Launch times	Effective balloon counts
Golmud	2780 m	Aug. 4 to Aug. 30, 2020	Around 07:30 am and 19:30 pm	45
Dunhuang	1140 m	Nov. 27 to Dec. 25, 2020	Around 07:30 am and 19:30 pm	50
Zhangye	1485 m	Nov. 27 to Dec. 25, 2020	Around 07:15 am and 19:15 pm	50

The self-developed radiosonde balloon system consists of launching and receiving parts, and the corresponding launching and receiving schematic circuit diagrams are shown in Fig. 1c (Cai et al., 2018). It mainly includes a micro temperature sensor, data measurement and conversion module, analog input port, digital input port, receiving power amplifier, host, and other components. The analog input port is mainly connected to the analog signal of the two-way temperature sensor, which is converted into a digital signal through the conditioning circuit and A/D (analog-to-digital conversion), so as to obtain the temperature structure constant C_{T}^2. The digital input port is connected to the digital signals of GPS and temperature, humidity and pressure modules to obtain radiosonde position information, the profile data of

https://doi.org/10.5194/amt-2021-55
Preprint. Discussion started: 18 March 2021

wind speed, wind direction, air temperature, relative humidity and pressure, respectively. The data measurement and conversion module performs unified coding of data format and baud rate, and transmits the signal through the antenna after secondary modulation of 32.8 kHz and 400 MHz. Received through the antenna, the signal enters the receiving system; then, after filtering and amplifying, the signal is converted in the receiver to obtain a 32.8 kHz signal, before then being amplified and demodulated by the serial port and finally sent to the computer for processing and storage. The response range of the micro temperature sensor is 0.1–30 Hz, so the minimum temperature fluctuation standard deviation of the corresponding measurement is ≤ 0.002℃.

2.2 Methods

For fully developed turbulence, it is assumed that Kolmogorov's locally uniform isotropic turbulence theory is satisfied(Kolmogorov, 1968). The relationship between the temperature structure constant C_{T}^2 and the temperature difference between two points in space (distance *r*) is as follows:

$$C_{\mathrm{T}}^2 = \langle [T(x) - T(x+r)]^2 \rangle r^{-2/3}, \tag{1}$$

where $l_0 \ll r \ll L_0$, in which l_0 and L_0 are the inner and outer scales of the turbulence, respectively; T is the atmospheric temperature (°C), and then $T(x)$ and $T(x+r)$ are the temperature of two points in space (distance r), respectively; and ⟨⟩ represents the ensemble average. The value of r is 1 m, which is the spatial distance between the two micro temperature sensors in this study. The core of the micro temperature sensor is a platinum wire with a diameter of about 20 μm and a resistance of about 10 Ω. The change of air temperature at two points in space sensed by the micro temperature sensor is ΔT, which is converted to electrical resistance change ΔV. ΔV is related to ΔT as follows:

$$\Delta V = A \cdot \Delta T, \tag{2}$$

where A is the calibration coefficient. C_{T}^2 can be obtained by substituting equation 2 into equation 1. In the visible and near-infrared wavelengths, the fluctuation of refractive index is mainly caused by temperature fluctuation, and the influence of relative humidity can be ignored. Therefore, the refractive index structure constant C_{n}^2 can be calculated as

$$C_n^2 = \left(7.9 \times 10^{-5} \frac{P}{T^2}\right)^2 C_{\mathrm{T}}^2. \tag{3}$$

According to the locally uniform isotropic theory, Tatarski obtained the relationship between measured meteorological parameters and the estimated C_n^2 as (Tatarski model) (Tatarski, 1961)

$$C_n^2 = \alpha L_0^{4/3} \left(-\frac{79 \times 10^{-6} P}{T^2} \frac{\partial \theta}{\partial h}\right)^2, \tag{4}$$

where α is a constant and the value is 2.8, L_0 is the outer scale of turbulence, θ is potential temperature (K), and $h$is height above ground (m). The conversion relationship between potential temperature θ and air temperature T is $\theta = T\left(\frac{1000}{P}\right)^{0.286}$. It can be found from equation 4 that the estimated value of C_{n}^2 can be obtained by substituting the measured meteorological parameters and the estimated L_0. Many researchers have proposed different C_{n}^2 profile models through long-term measurement and statistical analysis of different experimental sites. The widely used models for C_{n}^2 profile estimation are the AFGL (Air Fore Geophysics Laboratory) and Hufnagel–Vally models (Good et al., 1988; Hufnagel and

https://doi.org/10.5194/amt-2021-55
Preprint. Discussion started: 18 March 2021

Atmospheric Measurement Techniques
Discussions

Stanley, 1964; Rothman et al., 1983). The establishment of these types of models only relies on the average calculation and fitting to obtain the C_n^2 profiles. For example, the formula of the Hufnagel–Vally model (hereinafter referred to as the H-V model) is as follows (Cheng et al., 2013):

$$C_n^2(h) = 8.2 \times 10^{-1}\ W^2(h/10)^{10}\exp(-h) + 2.7 \times 10^{-1}\ \exp(-h/1.5) + A\exp(-h/0.1)$$
$$W^2 = \frac{1}{15}\int_5^{20} V^2(h)\mathrm{d}h \quad , \tag{5}$$

where W is the root-mean-square wind speed at a height 5–20 km (m/s), $V(h)$ is the wind speed at a certain height (m/s), and A is a parameter describing the intensity of atmospheric near-surface optical turbulence. The adjustable parameters W and A can be selected by fixing the isotropic angle and the coherence length. For example, when the observation wavelength is selected to be 500 nm, the isotropic angle is 7 μrad, the coherence length is 5 cm, and the corresponding A and W are $1.7 \times 10^{-14}\,\mathrm{m}^{-2/3}$ and 21 m/s, respectively. This type of C_n^2 profile model is a function of height and cannot show detailed changes in turbulence. Dewan et al. (1993), meanwhile, introduced wind shear into the outer-scale estimation (Dewan model), and Ruggiero et al. (2004) further introduced temperature gradients into their model, which is called HMNSP99. The empirical formula separately expresses the outer-scale L_0 according to the troposphere and stratosphere as

$$S = \left[\left(\frac{\partial u}{\partial h}\right)^2 + \left(\frac{\partial v}{\partial h}\right)^2\right]^{1/2}, \tag{6}$$

$$L_0^{4/3} = \begin{cases} 0.1^{4/3} \times 10^{0.362+16.728S-192.347\frac{\mathrm{d}T}{dh}}, & \text{Troposphere} \\ 0.1^{4/3} \times 10^{0.757+1\ \ .819S-\ \ .784\frac{\mathrm{d}T}{\mathrm{d}h}}, & \text{Stratosphere} \end{cases}, \tag{7}$$

where S is wind shear; u and v are radial wind speed and lateral wind speed, respectively; and $\mathrm{d}T/\mathrm{d}h$ is the vertical temperature gradient.

Comparison of C_n^2 profiles estimated by different outer models shows that high-altitude wind shear and temperature gradients may be the main factors that induce optical turbulence (Cai et al., 2018). Therefore, it is more realistic to associate outer-scale L_0 with high-altitude wind shear and temperature gradients. Based on the HMNSP99 model and combined with the observation results at the three sites, 56 radiosonde data with good signal reception and at least 28 km or more were selected for analysis. We refitted and obtained an outer-scale model that was well matched with the climate and environment of the three sites, which is referred to here as the improved model (equation 8). Inserting the improved model into equation (4), we obtain the estimated C_n^2 value as follows:

$$L_{Improved-mo}^{4/3} = \begin{cases} 0.1^{4/3} \times 10^{0.397+17.723S-179.226\frac{\mathrm{d}T}{dh}}, & \text{Troposphere} \\ 0.1^{4/3} \times 10^{0.612+1\ \ .675S-\ \ .287\frac{\mathrm{d}T}{\mathrm{d}h}}, & \text{Stratosphere} \end{cases}, \tag{8}$$

3. Optical turbulence measurement and model analysis

3.1 Measured results at three sites

For quantitative description, pseudo-color images of each profile are presented (Fig. 2), and the height of the observation data is 0–25 km. In this study, air pressure, temperature, wind direction, wind speed, relative humidity, and C_n^2 were statistically averaged every 30 m, and the corresponding profile's average value and standard deviation were obtained. In addition, unless otherwise stated, all altitudes refer to the altitude above ground level relative to the observation site, and the time is Beijing time.

https://doi.org/10.5194/amt-2021-55
Preprint. Discussion started: 18 March 2021

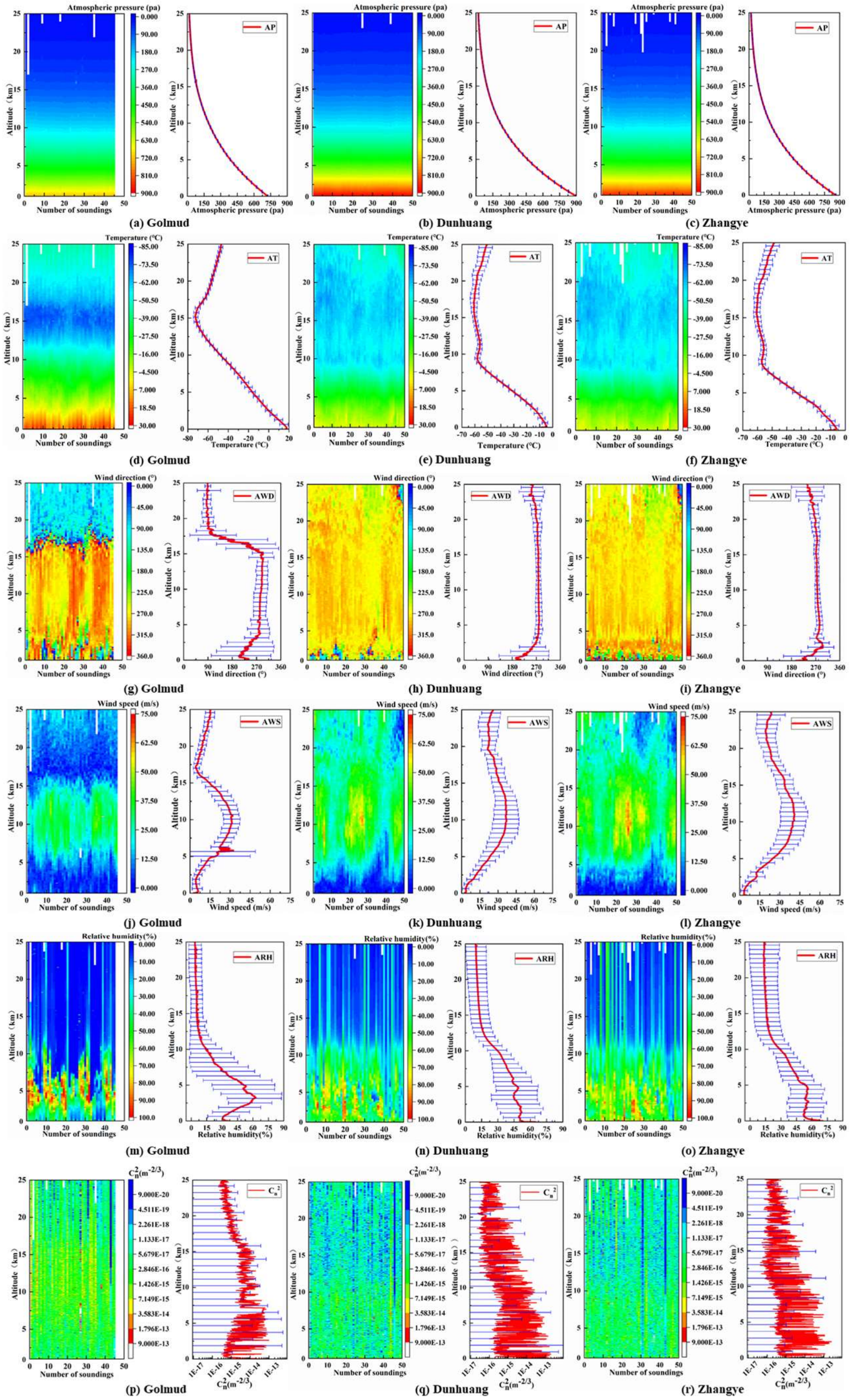

https://doi.org/10.5194/amt-2021-55
Preprint. Discussion started: 18 March 2021

Atmospheric Measurement Techniques Discussions
Open Access

Figure 2. Meteorological parameters measured by balloons at three different sites. Atmospheric pressure: (a) Golmud; (b) Dunhuang, (c) Zhangye. Temperature: (d) Golmud; (e) Dunhuang; (f) Zhangye. Wind direction: (g) Golmud; (h) Dunhuang; (i) Zhangye. Wind speed: (j) Golmud; (k) Dunhuang; (l) Zhangye. Relative humidity: (m) Golmud; (n) Dunhuang; (o) Zhangye. C_n^2: (p) Golmud; (q) Dunhuang; (r)Zhangye. The red single profile represents the average value of each parameter, and the blue line segment is the standard deviation.

In particular, it is noticeable that although Dunhuang and Zhangye are 513 km apart, the observational results of the two sites above 5 km were very similar (Figs. 2b–c, 2e–f, 2h–i, 2k–l, 2n–o, 2q–r). This indicates that there was a high consistency in the variability of the high-altitude meteorological parameters above 5 km at the two sites during the observation period (the time difference between the two sites to release the balloon was no more than 15 minutes). The difference below 5 km was caused by the different underlying surface and local climate conditions. It can be seen that the atmospheric pressure was gradually decreasing (Figs. 2a–c). During the observation period, the pressure was stable without obvious diurnal changes. In addition, the near-surface pressure of Dunhuang and Zhangye in winter was significantly higher than that of Golmud in summer. This might be closely related to the seasonal climate and terrain height.

Figs. 2d–f show that the tropopause of Golmud appeared at about 15 km, while the average temperature profiles of Dunhuang and Zhangye were similar, and there seemed to be more than one tropopause. After accurate calculation, it was found that, due to the averaging effect, multiple tropopauses (hereinafter referred to as MTs) were not obvious. During the observation period, the phenomenon of MTs occurred many times in Dunhuang and Zhangye. Two cases were selected from the observation data (Fig. 3): (a) the radiosonde data of Dunhuang from 19:17 to 20:49 on Nov. 27, 2020 showed that the positions of the first tropopause and the second tropopause were around 10 km and 16 km respectively, and the thickness of the tropopause was 6 km; and (b) the radiosonde data of Zhangye from 7:15 to 8:49 on Nov. 29, 2020 showed that the positions of the first tropopause and the second tropopause were around 10 km and 19.4 km respectively, and the thickness of the tropopause was 9.4 km.

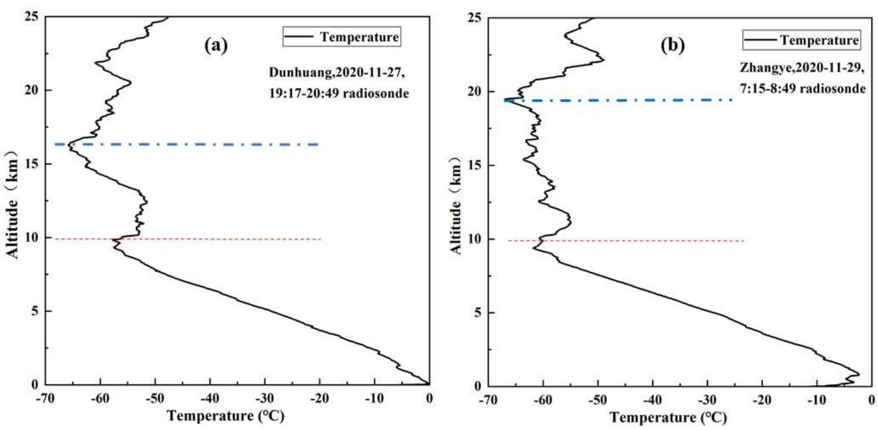

Figure 3. Multiple tropopause events: (a) Dunhuang, 2020-11-27, 19:17–20:49; (b) Zhangye, 2020-11-29, 7:15–8:49.

https://doi.org/10.5194/amt-2021-55
Preprint. Discussion started: 18 March 2021

Atmospheric Measurement Techniques Discussions

Figs. 2g–i and Figs. 2j–l show that: (1) During the summer observation period, southwesterly and westerly winds prevailed in the near-surface layer (0–5km) of Golmud, with an average wind speed below 20 m/s; westerly and northwesterly winds prevailed in the troposphere (5–15 km), at which level the wind speed was the highest, with a peak value of 40 m/s; and easterly and southeasterly winds prevailed in the stratosphere, where the average wind speed at a height of 17 km was at least 7 m/s, and then gradually increased. (2) During the winter observation period, the wind direction near the ground (0–3 km) in Dunhuang and Zhangye was changeable, most likely because of the influence of local topography (high mountains, Gobi deserts, etc.); the average wind speed was also small, below 10 m/s; westerly and northwesterly winds prevailed at altitudes above 3 km; and the maximum wind speed occurred at a height of 10 km, with a peak value of 75 m/s. This was a typical subtropical jet, and the abovementioned MTs usually formed under its influence.

Previous studies have shown that strongly developed deep convective systems influenced by the subtropical jet can penetrate the tropopause—that is, 'penetrating convection' (tropospheric air invading the stratosphere) (Fueglistaler et al., 2009; Randel and Jensen, 2013). The penetrating convection can not only transport air from the planetary boundary layer to the top of the troposphere, but also transport trace substances such as water vapor from the troposphere to the stratosphere via the tropopause, which in turn affects radiation and its budget in the upper troposphere and lower stratosphere (Emmanuel et al., 2021; Randel and Jensen, 2013; Sherwood and Dessler, 2000; Tegtmeier et al., 2020). Based on the observational results (Figs. 2u–o), the relative humidity of the stratosphere in Dunhuang and Zhangye reached more than 30% many times during the winter observation period, which provides practical evidence to verify the previous theory. In addition, the relative humidity was relatively high below 5 km (about 45%), which might be closely related to the special terrain of the Qinghai-Tibet Plateau and the semi-arid and semi-humid climate of the Qilian alpine zone.

The intensity of the high-altitude optical turbulence in the northwest was basically distributed at 10^{-19}–10^{-13} $m^{-2/3}$. The turbulence profiles (C_n^2) show that the strong turbulence of Golmud in summer appeared in the near-surface (0–5 km) and tropospheric (10–15 km) levels, the profiles above 10 km during the observation period were relatively uniform, and there were no big changes in magnitude (Figures 2p–r). The activities of various scales of turbulence could cause unstable stratification in the troposphere. In the stratosphere, the scale of turbulence was smaller and the stratification was more stable. In winter, the changes of turbulence in Dunhuang and Zhangye were abundant, and the temperature gradients near the ground (0–5 km) and in the upper troposphere (15–20 km) changed dramatically, which should correspond to the strong turbulence layer in Fig. 2. Due to the existence of penetrating convection, various scales of tropospheric turbulence can directly enter the stratosphere, resulting in big differences in the magnitude of turbulence when the profiles are averaged.

3.2 Comparative analysis of the H-V model and measurements

A total of 56 C_n^2 profile data from the three sites (including 19 data in Golmud, 22 data in Dunhuang, and 15 data in Zhangye) with good signal reception and a detection height of 28 km or more were selected. The data were averaged and smoothed, and retained to a height of 28.5 km. The measured values are shown in Fig. 4, and the intensity of turbulence is distributed in 10^{-17}–10^{-13} $m^{-2/3}$. At the same time, C_n^2 empirical models of the three sites were

https://doi.org/10.5194/amt-2021-55
Preprint. Discussion started: 18 March 2021

refitted based on the H-V model (the empirical models for Golmud, Dunhuang and Zhangye are $C_n^2 - G$, $C_n^2 - D$ and $C_n^2 - Z$, respectively):

$$C_n^2 - G = 2.88 \times 10^{-26} h^{19.45} \exp(-h/0.54) + 8.06 \times 10^{-15} \exp(-h/6.25) + 8.11 \times 10^{-15} \exp(-h/5.56), \quad (9)$$

$$C_n^2 - D = 2.98 \times 10^{-18} h^{14.88} \exp(-h/0.31) + 4.16 \times 10^{-15} \exp(-h/4.34) + 4.52 \times 10^{-1} \exp(-h/4.17), \quad (10)$$

$$C_n^2 - Z = 7.45 \times 10^{-1}\ h^{-0.48} \exp(-h/1.47) + 2.67 \times 10^{-16} \exp(-h/11.11) + 2.51 \times 10^{-16} \exp(-h/11.11), \quad (11)$$

where h is the height (km). These statistical models can reflect the general law of turbulence intensity changes at these three sites in northwestern China. The expressions of the models contain three terms: the first term represents the strong turbulence that often occurs in the tropopause; the second term represents the turbulence in the boundary layer; and the third term represents the turbulence in the free atmosphere.

It can be seen from Fig. 4 that the strong turbulence of Golmud in summer appeared in the near-surface (0–5 km) level and below 15 km in the troposphere, which was consistent with the previous measured results. The empirical models of Dunhuang and Zhangye reflect the change trend of the selected measured values. Through careful observation, we can find the difference with the overall data; especially, the strong turbulence information below 15 km in the troposphere in Zhangye was not reflected. This is because there were relatively few profiles that could represent the strong tropospheric turbulence information in the selected profile data.

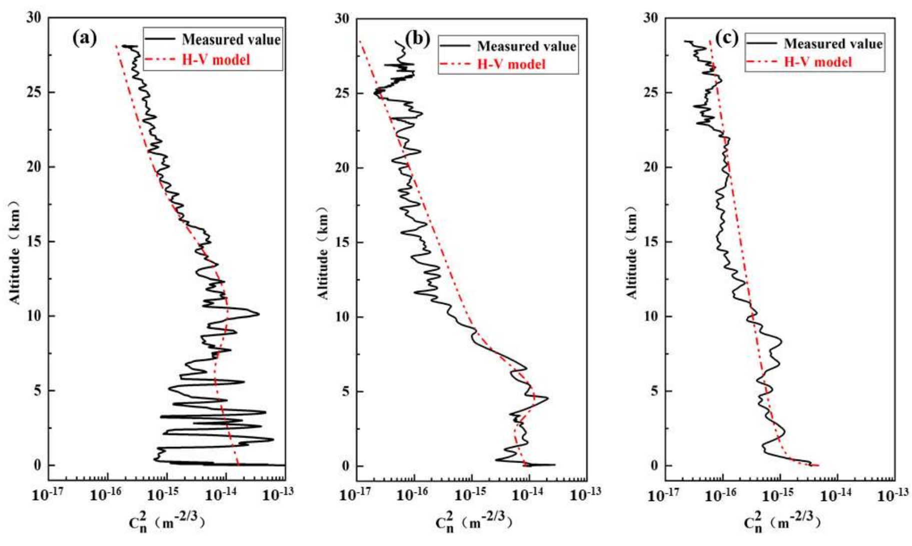

Figure 4. C_n^2 profiles from the H-V empirical model and measured values of three sites: (a) Golmud; (b) Dunhuang; (c) Zhangye.

3.3 Comparative analysis of the improved model and measured values

The overall trend of turbulence can be presented by the H-V model, but the detailed information of turbulence cannot be reflected. The measured meteorological parameters of observations were introduced into the improved model to obtain estimated values of C_n^2. From the above 56 profile data, two data of each site were randomly selected and recorded as

https://doi.org/10.5194/amt-2021-55
Preprint. Discussion started: 18 March 2021

Atmospheric Measurement Techniques Discussions

#1–6 balloon. The records of radiosonde balloons are shown in Table 2.

Table 2. Records of balloons at the three sites used in this study.

Balloon number		Launch date	Launch time	Termination time	Termination altitude (km)
Golmud	#1	Aug. 8, 2020	19:56	21:24	29.370
	#2	Aug. 13, 2020	7:35	8:55	30.330
Dunhuang	#3	Dec. 6, 2020	7:32	8:55	29.160
	#4	Dec. 7, 2020	19:33	20:57	30.840
Zhangye	#5	Dec. 3, 2020	19:15	20:36	28.950
	#6	Dec. 21, 2020	07:15	08:39	29.070

As shown in Fig. 5, the C_n^2 profiles estimated by the improved model were compared with the measured values for balloon #1–6. The results of balloon #1–2 (Figs. 5a–b) show that the turbulence above 15 km decreased gradually; the strong turbulence layer appeared below 15 km, and a peak value occurred at 10 km–15 km, reaching 10^{-13} m$^{-2/3}$ or more. This shows that below 15 km, the convection was strong, and the corresponding wind shear and temperature gradient changed drastically, which is consistent with the performance of Golmud's $C_n^2 - G$ model. The results of balloon #3–6 (Figs. 5c–f) show that the strong turbulence layer appeared below 15 km, with a peak value of more than 10^{-13} m$^{-2/3}$, and the magnitude of turbulence above 20 km was still 10^{-17} m$^{-2/3}$ or more; in particular, the turbulence of balloon #3 and #4 had increased above 20 km, which indicates that the occurrence of penetrating convection, and the drastic change of the wind shear and temperature gradients could be transported directly from the troposphere to stratosphere. This affected and changed the heat radiation and its budget in the lower stratosphere, and further changed the formation mechanism of turbulence. The improved model can better reflect the varied characteristics and formation mechanism of turbulence than the above-mentioned empirical models ($C_n^2 - D$ and $C_n^2 - Z$). In general, the C_n^2 profile estimated by the improved model is more consistent with the measured C_n^2 profile both in magnitude and overall trend, and the improved model can also capture details of turbulence at high altitude.

Fig. 6 shows the correlation between the C_n^2 values estimated by the improved model and the measured values for balloon #1–6. The coefficients of determination are 0.85, 0.84, 0.91, 0.85, 0.82 and 0.89 respectively, which shows that the improved model has a high degree of correlation with the measured values. Fig. 5 shows that the source of the differences are mainly concentrated in the lower stratosphere (20–25 km, Figs. 5b–e) and the troposphere below 10 km (Figs. 5a–e), which indicates that the meteorological parameters of the observation sites are significantly different in summer and winter: there was obvious horizontal wind shear near the height of 15 km at Golmud in summer, while the horizontal wind shear of Dunhuang and Zhangye in winter (Figs. 2g–h) only occurred frequently below 5 km. The temperature gradients at the three sites changed drastically below 10 km, while the difference was that the lower stratosphere of Dunhuang and Zhangye in winter changed drastically above 20 km, which was due to the occurrence of penetrating convection.

https://doi.org/10.5194/amt-2021-55
Preprint. Discussion started: 18 March 2021

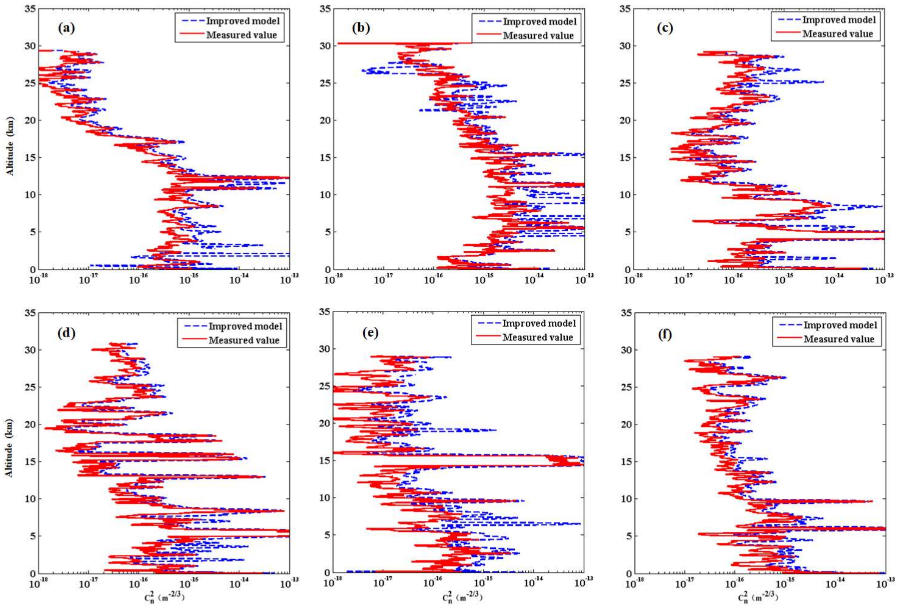

Figure 5. The refractive index structure parameter (C_n^2) from the improved model and measured values for balloon (a) #1, (b) #2, (c) #3, (d) #4, (e) #5, and (f) #6.

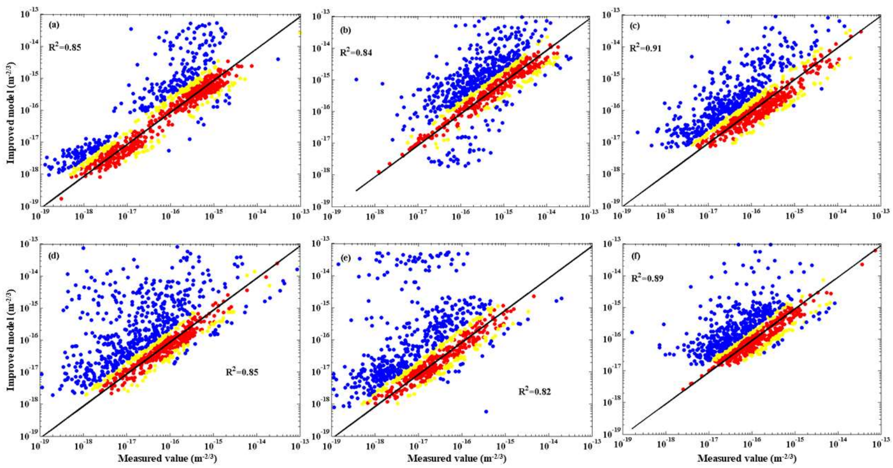

Figure 6. Scatter plots of the improved model and measured values for balloon (a) #1, (b) #2, (c) #3, (d) #4, (e) #5, and (f) #6. Blue, yellow and red colors indicate the dot density from low to high, respectively.

4. Conclusion

A self-developed radiosonde balloon system was used to conduct high-altitude optical turbulence observations at three sites in northwestern China. The intensity of the high-altitude optical turbulence in the northwest was basically distributed at 10^{-19}–10^{-13} $m^{-2/3}$. There were obvious differences in the high-altitude distribution characteristics of turbulence in summer and winter: the strong turbulence of Golmud in summer mainly appeared in the near-surface level and at a height below 15 km. In winter, there were large changes of optical turbulence at Dunhuang and Zhangye in terms of the magnitude of different levels; the subtropical jet caused the MTs of Dunhuang and Zhangye to appear at 10–20 km, and the resulting penetrating convection also changed the heat transfer and its budget at high altitude; the turbulence below the troposphere and planetary boundary layer was transported to the stratosphere; and the stratospheric wind shear and temperature gradients changed drastically, which made the turbulence in the stratosphere increase instead of decrease.

Based on the H-V model and HMNSP99 model, the empirical models (H-V empirical models) and the improved model were established separately by using the radiosonde data of the three sites. These models are consistent with the climate characteristics and turbulence variation law of the Qinghai-Tibet Plateau and Hexi Corridor in northwestern China. The empirical models and the improved model were compared with the measured values. It was found that the H-V empirical model can represent the general law and trend of turbulence development, while the detailed changes of each height layer will be ignored when using the H-V empirical model. In contrast, the improved model can reflect the detailed information of each level, and the correlation between the improved model and the measured values can be as high as 0.91 and as low as 0.82. This proves the correctness of introducing wind shear and temperature gradients to study changes in high-altitude turbulence. The improved model can be used for turbulence estimation and forecasting in northwestern China.

The H-V empirical models and the improved model in this study are mainly based on experiments and limited sounding data. Long-term accumulation of experience and continuous correction of a large amount of measured data are required to obtain a more universal turbulence parameter estimation model. Although the improved model can obtain detailed changes in high-altitude turbulence, there is still a slight deviation in the fine structure. According to the specific terrain and climate change characteristics, the introduction of more reasonable models of other factors, and the use of higher-precision acquisition sensors, will help us improve the accuracy of estimation.

Acknowledgments: This work was jointly funded by the Strategic Priority Research Program of Chinese Academy of Sciences (Grant No. XDA17040524), (Grant No. D040103, Grant No. 010567900) and Key Program of 13th five-year plan, CASHIPS, (Grant No. KP-2019-05). Thanks to the satellite imagery provided by Google Earth (https://map.bmcx.com/). Thanks to the National Meteorological Observatory of Golmud, Dunhuang and Zhangye for their support.

Author Contributions: Supervision, Chenbo Xie; Designed the study, Hao Yang; Methodology, Xu Deng, Hao Yang and Zhiyuan Fang; Software, Hao Yang, Cheng Li, Kunming Xing; Writing–original draft, Hao Yang; Writing–review & editing, Chenbo Xie and Hao Yang.

Conflicts of Interest: The authors declare no conflict of interest.

References

Basu, S.: A simple approach for estimating the refractive index structure parameter (C-n(2)) profile in the atmosphere, Optics Letters, 40, 4130-4133, 2015.

Bendersky, S., Kopeika, N. S., and Blaunstein, N.: Atmospheric optical turbulence over land in middle east coastal environments: prediction modeling and measurements, Applied Optics, 43, 4070-4079, 2004.

https://doi.org/10.5194/amt-2021-55
Preprint. Discussion started: 18 March 2021

Bi, C., Qian, X., Liu, Q., Zhu, W., Li, X., Luo, T., Wu, X., and Qing, C.: Estimating and measurement of atmospheric optical turbulence according to balloon-borne radiosonde for three sites in China, Journal of the Optical Society of America a-Optics Image Science and Vision, 37, 1785-1794, 2020.

Cai, J., Li, X.-B., Zhan, G.-W., Wu, P.-F., Xu, C.-Y., Qing, C., and Wu, X.-Q.: A new model for the profiles of optical turbulence outer scale and C-n(2) on the coast, Acta Physica Sinica, 67, 2018.

Cheng, Z., Hou, Z., Jing, X., Li, F., Lu, Q., and Yu, L.: High-precision and real-time inversion method of Hufnagel-Valley turbulence profile, Infrared and Laser Engineering, 42, 1562-1567, 2013.

Cherubini, T., Businger, S., Lyman, R., and Chun, M.: Modeling optical turbulence and seeing over Mauna Kea, Journal of Applied Meteorology and Climatology, 47, 1140-1155, 2008.

Dewan, E., Good, R., Beland, R., and Brown, J.: A Model for Csubn(2) (Optical Turbulence) Profiles Using Radiosonde Data, 1993. 50, 1993.

Emmanuel, M., Sunilkumar, S. V., Muhsin, M., Chandran, P. R. S., Parameswaran, K., Kumar, B. S., Maitra, A., Satyanarayana, A. N. V., and Nagendra, N.: Effect of monsoon dynamics and deep convection on the upper troposphere lower stratosphere water vapour over Indian monsoon region, Atmos Res, 249, 2021.

Fueglistaler, S., Dessler, A. E., Dunkerton, T. J., Folkins, I., Fu, Q., and Mote, P. W.: Tropopause Layer, Reviews of Geophysics, 47, 2009.

Good, R. E., Beland, R. R., Murphy, E. A., Brown, J. H., and Dewan, E. M.: Atmospheric models of optical turbulence, Proc. SPIE, 928, 165-186, 1988.

He, W.-g., Wu, J., Yang, C.-p., Han, Y., and Xu, G.-y.: Estimation and measurement of the optical turbulence over land, Journal of University of Electronic Science and Technology of China, 37, 893-896, 2008.

Hufnagel, R. E. and Stanley, N. R.: Modulation Transfer Function Associated With Image Transmission Through Turbulent Media, Journal of the Optical Society of America, 54, 52-&, 1964.

Hutt, D. L.: Modeling and measurements of atmospheric optical turbulence over land, Optical Engineering, 38, 1288-1295, 1999.

Kolmogorov, A. N.: Local Structure Of Turblence In An Incompressible Viscous Fluid At Very High Reynolds Numbers, Soviet Physics Uspekhi-Ussr, 10, 734-+, 1968.

Kornilov, V., Tokovinin, A., Shatsky, N., Voziakova, O., Potanin, S., and Safonov, B.: Combined MASS-DIMM instruments for atmospheric turbulence studies, Monthly Notices of the Royal Astronomical Society, 382, 1268-1278, 2007.

Osborn, J., Butterley, T., Townson, M. J., Reeves, A. P., Morris, T. J., and Wilson, R. W.: Turbulence velocity profiling for high sensitivity and vertical-resolution atmospheric characterization with Stereo-SCIDAR, Monthly Notices of the Royal Astronomical Society, 464, 3998-4007, 2017.

Randel, W. J. and Jensen, E. J.: Physical processes in the tropical tropopause layer and their roles in a changing climate, Nature Geoscience, 6, 169-176, 2013.

Rani, M., Bhatti, H. S., and Singh, V.: Analysis of Atmospheric Turbulence on Free Space Optical System using Homotopy Perturbation Method, Journal of Optical Communications, 40, 441-446, 2019.

Rothman, L. S., Gamache, R. R., Barbe, A., Goldman, A., Gillis, J. R., Brown, L. R., Toth, R. A., Flaud, J. M., and Camy-Peyret, C.: AFGL atmospheric absorption line parameters compilation: 1982 edition, Appl Opt, 22, 2247-2256, 1983.

Ruggiero, F., DeBenedictis, D., Lefevre, R., and Early, S.: Mesoscale modeling effects on optical turbulence parameterization performance, B Am Meteorol Soc, 2004. 2004.

Sherwood, S. C. and Dessler, A. E.: On the control of stratospheric humidity, Geophys Res Lett, 27,

https://doi.org/10.5194/amt-2021-55
Preprint. Discussion started: 18 March 2021

2513-2516, 2000.

Tatarski, V.: Wave Propagation in a Turbulent Medium, 1961.

Tegtmeier, S., Anstey, J., Davis, S., Ivanciu, I., Jia, Y., McPhee, D., and Kedzierski, R. P.: Zonal Asymmetry of the QBO Temperature Signal in the Tropical Tropopause Region, Geophys Res Lett, 47, 2020.

Travouillon, T., Schoeck, M., Els, S., Riddle, R., and Skidmore, W.: Using a Sodar to Measure Optical Turbulence and Wind Speed for the Thirty Meter Telescope Site Testing. Part II: Comparison with Independent Instruments, Boundary-Layer Meteorology, 141, 289-300, 2011.

Vanzandt, T. E., Gage, K. S., and Warnock, J. M.: An Improved Model for the Calculation of Profiles of Cn2 and Epsilon in the Free Atmosphere from Background Profiles of Wind, Temperature, and Humidity, B Am Meteorol Soc, 62, 924-924, 1981.

Wang, H., Yao, Y., and Liu, L.: Forecast of Atmosphere Optical Turbulence at Ali Site by Weather Research and Forecasting Model, Acta Optica Sinica, 33, 0301006-0301001-0301006-0301005, 2013.

Wu, S., Hu, X., Han, Y., Wu, X., Su, C., Luo, T., and Li, X.: Measurement and analysis of atmospheric optical turbulence in Lhasa based on thermosonde, Journal of Atmospheric and Solar-Terrestrial Physics, 201, 2020a.

Wu, S., Su, C., Wu, X., Luo, T., and Li, X.: A Simple Method to Estimate the Refractive Index Structure Parameter (Cn2) in the Atmosphere, Publications of the Astronomical Society of the Pacific, 132, 2020b.

Wu, X.-q., Sun, G., Weng, N.-q., Xiao, L.-m., Xu, L.-m., Lu, W.-y., Xu, A.-l., and Nie, Q.: Measurement and modeling of Cn2 at typical regions in China, Journal of Atmospheric and Enviromental Optics, 2, 409-422, 2007.